Phase relations in a photonic 4-dimensional Hadamard gate – a non-polarizing beamsplitter

A. Kryvobok, *FLIR Systems Inc.*, A.D. Kathman, *FLIR Systems Inc.*

***Abstract*—Beamsplitter is often given as a matrix acting on a vector with two basis states. This might be comprehensive for a scalar field but certainly insufficient in case of photons which are vector fields. In this paper we discuss theoretical grounds to accurately define elements of a beamsplitter 4-matrix accounting for transverse polarization modes and provide experimental evidence confirming the predictions. Our theoretical approach involves certain non-classical conditions. Such feature makes this discussion curious from the scientific point of view since we conduct our experiment with coherent – classical fields. We propose an application of the beamsplitter in a field of quantum computing.**

***Index Terms*—Beamsplitter, optical interferometry, quantum computing**

I. Introduction

QUANTUM computing is noticeably popular and attractive field of active research. Remarkably quantum computation may be performed involving a variety of physical fields including photonics. It would therefore appear we could modestly contribute to quantum computing with our study on properties of a polarization independent beamsplitter. A beamsplitter transforming an input optical fields into a superposition of several optical fields is in essence a Hadamard transformation in terms quantum computing. There exists a well-established matrix representation for 2-dimensional optical beamsplitter which is used as a Hadamard logical gate producing a superposition of two spatial output modes. Extending the superposition space to higher dimensions would be a natural goal of quantum computing in order to increase the computational power. In this respect photonics can offer an upscale by introduction of polarization modes. To pay an account to prior art we considered studies on quantum mechanical description of a beamsplitter involving polarization modes [1] and [5], yet the formalism proposed in these papers would disagree with our findings.

In our work we discuss theoretical deduction and experimental verification of a 4-dimensional transformation matrix representation for the unpolarized lossless beamsplitter. The derived four by four matrix spans 4-dimensional Hilbert space with two spatial and two orthogonal polarization modes and represents an appropriate amplitude distribution for these modes.

The proposed representation in particular contributes to an exact phase distribution for resulting superposed fields which is of importance in terms of accurate estimation of quantum interference in quantum computing circuits. Such matrix, to the best of our knowledge, was not deduced explicitly before. Moreover, trivial expansion to 4-dimensions from a 2-dimensional beamsplitter according to Sylvester-Hadamard formalism [2] results in an expression which disagrees with the experiment. It feels therefore obligatory to mention that we refer to its action as a photonic Hadamard-like transformation resulting in a superposition state which is of use in quantum computing operations. This should not be confused with a proper Hadamard transformation formalism used, for example, in imaging [3].

The experimental setup which we used for a verification was significantly inspired by the Mach-Zehnder based simple quantum eraser discussed in the paper by Sneider et al. (2001) [4]. We certainly borrowed their approach to describe classical fields in a quantum mechanical picture. This is an elegant approach for an interference type experiments involving investigation of the polarization states of light. It is also a valid approach to emulate a single-photon interference statistics. By splitting the classical light into two parts the Mach-Zehnder introduces a definite phase relation between the parts. The split fields can hence be considered in a normalized manner as a vector with equivalent to a single-photon basis states. The action of optical instruments in such case, e.g. beamsplitter is merely about distribution of amplitudes for any operator governing the photon modes, i.e. be it coherent, chaotic light or single-photon statistics. Hence, the developed 4-dimensional photonic Hadamard-like transformation is applicable to single-photon based quantum computing operations.

II. Theoretical setup

Theoretical approach towards the sought beamsplitter matrix is based upon a pre-experimental and a post-experimental ansatz. Thus, prior to the experiment we followed common formalities – considering the matrix as a transformation matrix for arbitrary fields having two orthogonal polarization modes. The generalization of the fields allows easy 4-dimensional Hilbert space representation of their state vectors, namely having two spatial modes with two polarization modes. For the

Manuscript received June 5, 2019. This work was supported by our FLIR Systems Inc. colleagues: Lode Caenepeel, Jay James and Bill Terre.

Artem Kryvobok is with the FLIR Systems Inc., 27700 Parkway Avenue, Wilsonville, OR 97070 USA (e-mail: artem.kryvobok@flir.com).

Alan D. Kathman is with the FLIR Systems Inc., 27700 Parkway Avenue, Wilsonville, OR 97070 USA (e-mail: alan.kathman@flir.com).

transformation of the state vectors we adopted the matrix form of a polarization dependent beamsplitter given by expression (1) [5]. The ansatz aim is therefore to derive this matrix coefficients explicitly. It is worth noting that an unpolarized beamsplitter we investigate is not treated as simply polarization independent device but rather a partial case of a polarization dependent expression. Hence, coefficients of the matrix (1) are chosen to equally transmit and reflect the different polarization modes.

$$\begin{pmatrix} t_v & r_v & 0 & 0 \\ r_v & t_v & 0 & 0 \\ 0 & 0 & t_h & r_h \\ 0 & 0 & r_h & t_h \end{pmatrix} \quad (1)$$

The constituting matrix coefficients t_v, t_h, r_v, r_h are amplitudes for transmission of vertical and horizontal polarization and reflection of vertical and horizontal polarization accordingly. For polarization independence we set magnitudes of the amplitudes equal: $|t_v| = |t_h| = |r_v| = |r_h|$. Since there is no birefringence assumed within a beamsplitter we also set zero relative phase between t_v and t_h, so for a simplicity: $t_v = t_h = t$. Moreover, since no phase shift is deemed to occur for either mode upon the transmission we can safely let $t > 0, t\epsilon\mathbb{R}$. In this case, the phase of t can comfortably be treated as the frame of reference for phase relations within the matrix. Going forward, the experiment results suggested reflection amplitudes for the same polarization state of different spatial modes are not necessarily equal. Hence, as a part of the post-experimental ansatz we set r_v and $\widetilde{r_v}$ be the reflection amplitudes of different ports for vertical polarization and r_h and $\widetilde{r_h}$ – the reflection amplitudes of different ports for horizontal polarization accordingly. Further, we let relative phases of r_v, $\widetilde{r_v}$, r_h and $\widetilde{r_h}$ belong to the complex space with respect to t. Consequently, the resulting matrix is of the following form:

$$B = \begin{pmatrix} t & r_v & 0 & 0 \\ \widetilde{r_v} & t & 0 & 0 \\ 0 & 0 & t & r_h \\ 0 & 0 & \widetilde{r_h} & t \end{pmatrix} \quad (2)$$

A physical representation of input and output ports of a beamsplitter is shown on Fig. 1.

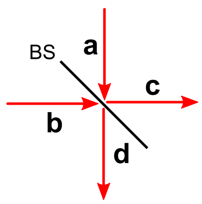

Fig. 1. Input and output ports in a beamsplitter.

We, hence, define the input state as:

$$|\psi_{in}\rangle = \begin{pmatrix} a_v \\ b_v \\ a_h \\ b_h \end{pmatrix} \quad (3)$$

where observing $\langle\psi_{in}|\psi_{in}\rangle = 1$, a_v and a_h are normalized amplitudes for vertical and horizontal polarizations in the input port a and b_v and b_h are normalized amplitudes for vertical and horizontal polarizations in the input port b accordingly. The output state is then obtained by B acting on the input state:

$$|\psi_{out}\rangle = B|\psi_{in}\rangle = \begin{pmatrix} c_v \\ d_v \\ c_h \\ d_h \end{pmatrix} = \begin{pmatrix} ta_v + r_v b_v \\ \widetilde{r_v} a_v + tb_v \\ ta_h + r_h b_h \\ \widetilde{r_h} a_h + tb_h \end{pmatrix} \quad (4)$$

where amplitudes c_v, c_h, d_v and d_h of the corresponding output ports c and d are as well normalized to satisfy $\langle\psi_{out}|\psi_{out}\rangle = 1$. Now, following the common thread of conservation of energy condition a lossless beamsplitter should perform a unitary transformation requiring:

$$|\psi_{in}|^2 = |\psi_{out}|^2 \quad (5)$$

The expressions (4) and (5) lead to explicit unitarity condition for a beamsplitter:

$$|\psi_{out}|^2 = \langle\psi_{in}|B^\dagger B|\psi_{in}\rangle \quad (6)$$

where (6) can only be satisfied if:

$$B^\dagger B = I_4 \quad (7)$$

with I_4 being an identity 4-matrix. The equation (7) leads to the following set of equations which are sometimes referred to as reciprocity relations [6]:

$$|t|^2 + |\widetilde{r_v}|^2 = 1 \quad (8,a)$$

$$|t|^2 + |r_v|^2 = 1 \quad (8,b)$$

$$|t|^2 + |\widetilde{r_h}|^2 = 1 \quad (8,c)$$

$$|t|^2 + |r_h|^2 = 1 \quad (8,d)$$

$$t^* r_v + \widetilde{r_v}^* t = 0 \quad (8,e)$$

$$r_v^* t + t^* \widetilde{r_v} = 0 \quad (8,f)$$

$$t^* r_h + \widetilde{r_h}^* t = 0 \quad (8,g)$$

$$r_h^* t + t^* \widetilde{r_h} = 0 \quad (8,h)$$

Recapping on the amplitudes conditions set out earlier: $t > 0, t\epsilon\mathbb{R} \Rightarrow |t_v| = |t_h| = t; t = |r_v| = |r_h|$ and $r_v, \widetilde{r_v}, r_h, \widetilde{r_h} \epsilon\mathbb{Z}$ we obtain the following set of possible solutions satisfying (8, a-h):

$$r_v = \widetilde{r_v} = \frac{\pm i}{\sqrt{2}} = \frac{\mp i}{\sqrt{2}};\ r_h = \widetilde{r_h} = \frac{\pm i}{\sqrt{2}} = \frac{\mp i}{\sqrt{2}};$$

and

$$r_v = \frac{\pm 1}{\sqrt{2}};\ \widetilde{r_v} = \frac{\mp 1}{\sqrt{2}};\ r_h = \frac{\pm 1}{\sqrt{2}};\widetilde{r_h} = \frac{\mp 1}{\sqrt{2}}.$$

Obviously, because the amplitudes $r_v, \widetilde{r_v}$ and $r_h, \widetilde{r_h}$ are not correlated the degree of degeneracy for these solutions is increased even further. Namely, there can be eight different solutions satisfying expressions (8,a-h). However, as it was mentioned earlier the experimental evidence imparted certain correlation between r_v and $\widetilde{r_v}$, r_h and $\widetilde{r_h}$ as well as cross correlation of reflection amplitudes for different polarization states. Thus, not all of the above solutions agree with the experiment implying certain weakness of sole condition of conservation of energy. This urged us to introduce an additional ansatz derived to explicitly require that output fields are orthogonal with respect to transverse modes. Such condition would impose a correlation between amplitudes $r_v, \widetilde{r_v}$ and $r_h, \widetilde{r_h}$ and it is because of this we denote them differently for different spatial modes. It is worth noting that this seemingly trivial approach from the point of view of classical physics has a strong validity in terms of quantum mechanics. The output fields in ports c and d contain coupling amplitudes of the input fields ports a and b which upon projection produce interfering cross terms that have to be suppressed as we shall see further. Following the definition (4) the orthogonal transverse components of the output state $|\psi_{out}\rangle$ are:

$$\left|\psi_{out_v}\right\rangle = \begin{pmatrix} c_v \\ d_v \end{pmatrix} = \begin{pmatrix} ta_v + r_v b_v \\ \widetilde{r_v} a_v + t b_v \end{pmatrix} \tag{9,a}$$

$$\left|\psi_{out_h}\right\rangle = \begin{pmatrix} c_h \\ d_h \end{pmatrix} = \begin{pmatrix} ta_h + r_h b_h \\ \widetilde{r_h} a_h + t b_h \end{pmatrix} \tag{9,b}$$

Hence, when projecting $\left|\psi_{out_v}\right\rangle$ onto $\left|\psi_{out_h}\right\rangle$ orthogonality holds if correspondingly: $\left\langle\psi_{out_v}\middle|\psi_{out_h}\right\rangle = \left\langle\psi_{out_h}\middle|\psi_{out_v}\right\rangle = 0$, which yields the following identity:

$$t^2 a_v^* a_h + t^* r_h a_v^* b_h + r_v^* t b_v^* a_h + r_v^* r_h b_v^* b_h + \widetilde{r_v}^* \widetilde{r_h} a_v^* a_h + \widetilde{r_v}^* t a_v^* b_h + t^* \widetilde{r_h} b_v^* a_h + t^2 b_v^* b_h = 0 \tag{10}$$

Equating coefficients of like terms results in the following equations:

$$t^2 + \widetilde{r_v}^* \widetilde{r_h} = 0 \tag{11,a}$$

$$t^* r_h + \widetilde{r_v}^* t = 0 \tag{11,b}$$

$$r_v^* t + t^* \widetilde{r_h} = 0 \tag{11,c}$$

$$r_v^* r_h + t^2 = 0 \tag{11,d}$$

Now we clearly obtained the correlations between the amplitudes $r_v, \widetilde{r_v}$ and $r_h, \widetilde{r_h}$ and consequently can add another restriction to the original degree of degeneracy. As per initial conditions these expressions have the following solutions, which we will expand to all possible permutations:

$$if\ r_h = \widetilde{r_h} = \frac{-i}{\sqrt{2}}\ and\ r_v = \widetilde{r_v} = \frac{i}{\sqrt{2}};$$

or

$$if\ r_h = \widetilde{r_h} = \frac{i}{\sqrt{2}}\ and\ r_v = \widetilde{r_v} = \frac{-i}{\sqrt{2}};$$

or

$$if\ r_h = \frac{-1}{\sqrt{2}}\ and\ \widetilde{r_h} = \frac{1}{\sqrt{2}}\ and\ r_v = \frac{1}{\sqrt{2}}\ and\ \widetilde{r_v} = \frac{-1}{\sqrt{2}};$$

or

$$if\ r_h = \frac{1}{\sqrt{2}}\ and\ \widetilde{r_h} = \frac{-1}{\sqrt{2}}\ and\ r_v = \frac{-1}{\sqrt{2}}\ and\ \widetilde{r_v} = \frac{1}{\sqrt{2}}.$$

Hence, our ansatz for the sought matrix representation can take any form from the following set of matrices:

$$B = \frac{1}{\sqrt{2}} \begin{pmatrix} 1 & -i & 0 & 0 \\ -i & 1 & 0 & 0 \\ 0 & 0 & 1 & i \\ 0 & 0 & i & 1 \end{pmatrix} \tag{12,a}$$

$$B = \frac{1}{\sqrt{2}} \begin{pmatrix} 1 & i & 0 & 0 \\ i & 1 & 0 & 0 \\ 0 & 0 & 1 & -i \\ 0 & 0 & -i & 1 \end{pmatrix} \tag{12,b}$$

$$B = \frac{1}{\sqrt{2}} \begin{pmatrix} 1 & -1 & 0 & 0 \\ 1 & 1 & 0 & 0 \\ 0 & 0 & 1 & 1 \\ 0 & 0 & -1 & 1 \end{pmatrix} \tag{12,c}$$

$$B = \frac{1}{\sqrt{2}} \begin{pmatrix} 1 & 1 & 0 & 0 \\ -1 & 1 & 0 & 0 \\ 0 & 0 & 1 & -1 \\ 0 & 0 & 1 & 1 \end{pmatrix} \tag{12,d}$$

All of the above expressions agree with our experiment, i.e. relative intensity phase and oscillation amplitude. Nonetheless, looking beyond the scope of our experiment further work may be suggested to narrow down the number of solutions. E.g. reproducing the Hong-Ou-Mandel (HOM) effect [13]. The original experiment and underlying formalism does not involve polarization states and it may as well be that with this additional degree of orthogonality the HOM experiment would run with different detection statistics. We have modeled the experiment with particular polarization states and found that expressions (12,a) and (12,b) may qualify to resemble a pattern of HOM experiment. One of the modeling examples is given in Annex I.

III. Experimental setup and results

In order to test the derived matrix expressions the input state of a beamsplitter should be prepared to have two spatial modes with definite initial phase as well as various combinations of polarization modes. Generally speaking, any two spatial input modes with correlated relative phase and controlled polarization modes satisfy the required input state. From a practical point of view, however, the easiest solution to both prepare the input state accordingly and test a beamsplitter action can be accomplished by the Mach-Zehnder interferometer (MZ) with a single coherent input. The part of such MZ just before a recombing beamsplitter provides two spatial modes with correlated relative phase and controlled polarization modes effectively prepares the input state as necessary while a recombing beamsplitter plays a role of a test beamsplitter. The details of our MZ experimental setup are shown on Fig. 2. In this setup we investigate the correlations of intensity oscillations of output arms from the ports 4 and 5 of MZ. The oscillations allow fully defining the output state and hence determine unambiguously an action of a beamsplitter upon the input state, i.e. the exact phase and amplitude relations within the beamsplitter matrix.

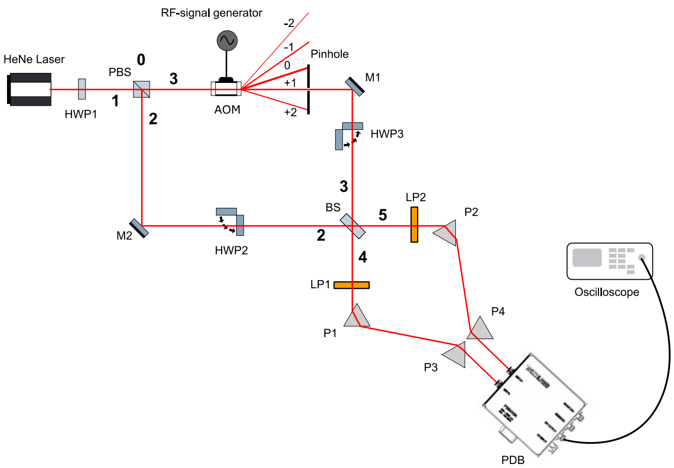

Fig. 2. Experimental setup testing the ansatz of beamsplitter matrix.

As a single coherent input we used 5 mW HeNe laser at 632.8 nm. The laser was specified to have linearly polarized Gaussian profile beam with linewidth of 1.8 MHz. This ensured a sufficient coherence length of several meters. Past the HeNe we inserted the first half-wave plate (HWP1) so to ease the control of linear polarization of the beam before MZ. The beam enters MZ in the polarizing beamsplitter (PBS) which transmits horizontally polarized component (port 2) of the beam and reflects the vertical one (port 3). The PBS features the extinction ratio of 1:1000 according to specifications, so for our laser power we can expect a substantial polarization purity in our measurements. In order to introduce a regular phase oscillation we inserted an acousto-optic modulator (AOM) in horizontally polarized arm of MZ. This ensured continuous oscillation in RF-band, so lower frequency oscillations caused by ambient lab vibrations and thermal changes did not influence our measurements. The choice of polarization in this case was rather arbitrary. We drove the AOM with the RF-signal generator being a voltage controlled oscillator (VCO) with a subsequent amplifier. With the help of voltage fed to the VCO and the amplifier we were able to tune the signal to a fixed frequency of about 107 MHz with 24 V peak-to-peak voltage. This provided the required power of acoustic beam inside the AOM to achieve sufficient diffraction efficiency. The particular optical beam and the AOM model parameters lead to operating in the Raman-Nath acousto-optic regime [7] producing several output diffraction orders. The diffracted beams are shifted in frequency equivalent to the diffraction order, i.e. 107 MHz multiple of: -2, -1, 0, +1, +2. For our measurements we chose the +1 order, i.e. up-shifted by about 107 MHz respecting the source beam. Since intensity fluctuations investigated are caused by beat the -1 order could have been equally chosen. We placed a pinhole with variable iris in the selected diffracted beam to isolate it for further alignment. The pinhole opening was slightly smaller than resulting beam diameter. Thus, due to Gaussian intensity distribution of wave front we could ensure bullseye interference alignment when beat amplitude was at highest amplitude. The AOM's higher diffraction orders were not a convenient choice due to reduction in intensity level as per Bessel distribution as well as requiring faster measuring instruments. The resulting arms of MZ were directed by mirrors M1 and M2 to recombine at non-polarizing 50:50 splitting ratio beamsplitter (BS). Each inner arm of MZ could have been switched to different polarization state by insertion of half-wave plates HWP2 and HWP3. The HWP2 and HWP3 had their fast axis (FA) set at $\frac{\pi}{4}$ rad. Thus upon insertion of HPW2 or HWP3 we could obtain: both vertical; both horizontal states; and swapping the states by inserting both waveplates before the recombination in BS. Further, past BS we set two linear polarizers: LP1 and LP2, i.e. in ports 4 and 5 accordingly. The relative orientations of the LP1 and LP2 axes played role in measuring phase amplitudes in our experiment. Thus, when taking measurements with two arms polarized orthogonally by setting the linear polarizers axes at $\frac{\pi}{4}$ rad or $-\frac{\pi}{4}$ rad we could superpose diagonal components of orthogonal states leading to interference and producing temporal intensity fluctuations. When HWP2 or HWP3 was inserted in either arm shifting them to the same polarization state LP1 and LP2 were set both accordingly to either vertical or horizontal position, so to achieve maximum transmission level, i.e. both at either 0 or $\frac{\pi}{2}$ rad. Hence, the above discussed HWP2, HWP3, LP1 and LP2 configurations produced beat on output arms 4 and 5. The correlations of beat intensities were observed by sending output beams individually into two P-i-N type photodetectors (PD). The output arms were steered at normal incidence to PD's inputs using arrangements of equilateral dispersive prisms P1, P2 and anamorphic prisms P3 and P4 as shown on Fig.2. The prisms were mounted onto kinematic mounts with azimuthal and polar degrees of freedom so beams could be conveniently aligned with PD's surfaces. The equilateral prisms provided a necessary sharp deviation angle which helped placing PD's in a compact manner yet the prisms suffered some polarization selectivity. As we study the action of unpolarized BS this adds a certain degree of complexity. According to the manufacturer specifications about 27% of transverse electric (TE) mode intensity [8] is reflected from the surface of the prism, so we correlated vertical component of a field amplitude to a factor of $\sqrt{0.73}$ per surface in our calculations. The second bend step was accomplished with anamorphic prisms featuring sufficient deviation and not having any polarization selectivity. The two PD's were housed inside balanced amplified photodetector (PBD). We used the Thorlabs fixed gain PDB410A model PBD with 100 MHz bandwidth suitable for modulation frequency of the AOM. It is important to emphasize that using a PBD detection is an essential part of the experiment in terms of providing an unambiguous phase correlation of output beams. This is due to an accurate spatial match and match of response time of both PD's. The PBD had two PD's photocurrent outputs coupled into a single RF output. One of the PD's operated in reverse bias ("input -") while the other in forward bias ("input +"). Hence, the PD's generated photocurrent in opposite directions relative to each other. In such a way when two beams of the same intensity are shone upon the PD's their individual photocurrents cancel each other out and the resulting current output is 0. Conversely, when there is an intensity difference the current level shifts to either negative or positive side depending on the PD bias direction. The PBD output was connected to a digital oscilloscope with 200 MHz spectral bandwidth, which fully accommodated our modulation frequency.

The experiment began with a pre-measurement sequence including overall MZ alignment and, in particular, the following steps:

1. Achieving symmetric photocurrent response from the two PD's. This step was performed with HWP2, HWP3, LP1 and LP2 removed. So, output BS arms contained both polarization states but did not interfere. The prisms P1, P2, P3 and P4 were then aligned with respect to PD's inputs till the point when we observed 0 current level on the oscilloscope in AC mode;
2. Balancing the intensity of vertical and horizontal polarization within MZ. This step is necessary since by default we recombine uneven intensities because only a single AOM diffraction order is used. To equalize the intensities we placed the PBD in port 5 before P2, P4 and LP1 exposing a single PD only to the output beam and consequentially blocked either arm of MZ. The HWP1 FA was then adjusted until we observed equal voltage response of the oscilloscope in DC mode;
3. Fine-tune alignment of prisms P1, P2, P3 and P4. In this step we ensure the oscillation depth is equivalent for both PD's. The PBD is placed to initial position as shown on Fig. 2 and by consequentially blocking either PD we align the prisms so that photocurrent oscillations from each PD are equal in amplitude;
4. Ensuring optical path difference (OPD) from port 4 to a PD and from port 5 to another PD is minimized. The correlation of beat phases is affected by relative path lengths of the output beams. The optical path lengths (OPL) are determined by relative position of prisms P1, P2, P3 and P4. These can be placed to form arbitrarily equal OPL's since beat cycle length is well over 1 meter. I.e. at 107 MHz modulation we have a period of full cycle of roughly 10 ns during which beam travels about 3 meters. Thus, spatial intensity change from 0 to maximum level is approximately every 1.5 m. Obviously, this ensures a rather large tolerance in physical position of the prisms which makes use of a simple ruler a sufficient precision. Placement of the prisms to form equal OPL's according to the ruler is then verified with modulation depth on the oscilloscope. With two arms being vertically polarized their intensities oscillate out of phase and therefore we observe an oscillation amplitude equivalent to double the magnitude respecting a single PD. The prisms can be then repositioned to fine-tune minimum OPD, i.e. to obtain the highest oscillation depth. In practice, however, a difference in OPL of even 10 cm does not produce any noticeable change and we mention this step as a general experimental formality.

Upon completion of these steps we proceed with the correlations tests. These measurements were performed for all possible polarization configurations in order fully test the ansatz on BS matrix. Namely, the following arrangements of optical instruments to which we will refer as six test configurations throughout this paper:

1. HWP2 is inserted with FA at $\frac{\pi}{4}$ rad and both the LP dials are set at $\frac{\pi}{2}$ rad (horizontally). In this configuration both arms are in horizontal state and interfere when recombined in BS;
2. HWP3 is inserted with FA at $\frac{\pi}{4}$ rad and both the LP dials are set at 0 rad (vertically). In this configuration both arms are in vertical state and interfere when recombined in the BS;
3. Both LP dials set at $\frac{\pi}{4}$ rad respecting the output ports of BS and with neither HWP2 nor HWP3 inserted. In this configuration horizontal and vertical polarizations are recombined and their diagonal components are set to interfere;
4. Oppositely set LP dials with one at $\frac{\pi}{4}$ rad and another at $-\frac{\pi}{4}$ rad with respect to the output ports of the BS and again without HWP2 and HWP3 inserted. In this configuration we achieve same situation as in previous step but with relative interference phase shifted by π;
5. Swapping polarization states between arms 2 and 3 by inserting both HWP2 and HWP3 and applying same LP setup as in test 3;
6. Swapping polarization states between arms 2 and 3 by inserting both HWP2 and HWP3 and applying same LP setup as in test 4.

The six configurations can be summarized in the following Table I.:

TABLE I.
SUMMARY OF TEST CONFIGURATIONS

Test configuration	Waveplates		Resulting state before the recombination in beamsplitter		Position of linear polarizers, rad	
	HWP2	HWP3	Arm 2	Arm 3	LP1	LP2
1	in	out	Horizontal	Horizontal	$\frac{\pi}{2}$	$\frac{\pi}{2}$
2	out	in	Vertical	Vertical	0	0
3	out	out	Vertical	Horizontal	$\frac{\pi}{4}$	$\frac{\pi}{4}$
4	out	out	Vertical	Horizontal	$\frac{\pi}{4}$	$-\frac{\pi}{4}$
5	in	in	Horizontal	Vertical	$\frac{\pi}{4}$	$\frac{\pi}{4}$
6	in	in	Horizontal	Vertical	$\frac{\pi}{4}$	$-\frac{\pi}{4}$

The results of measurements of these configurations are provided on the following figures which are screenshots from the oscilloscope.

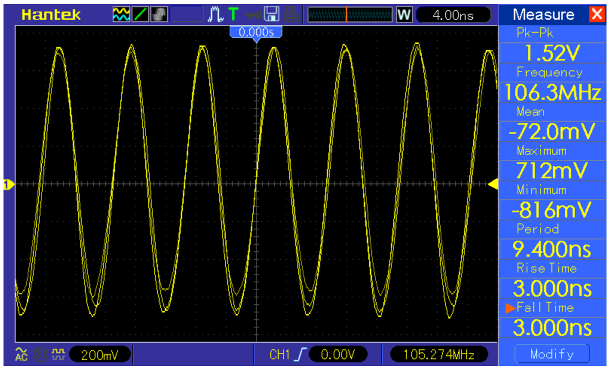

Fig. 3.1. Oscillation amplitude with both arms recombined in the horizontal state with LP1 and LP2 set at $\frac{\pi}{2}$ rad.

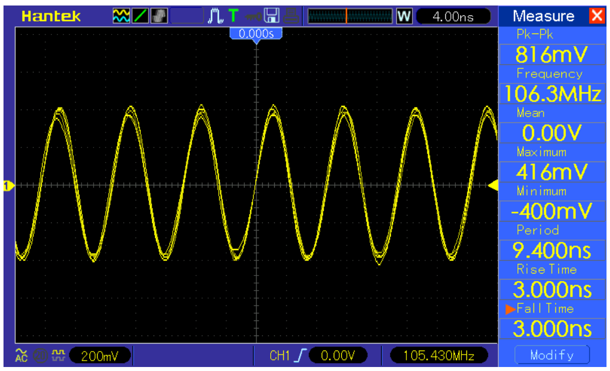

Fig. 3.2. Oscillation amplitude with both arms recombined in the vertical state with LP1 and LP2 set at 0 rad.

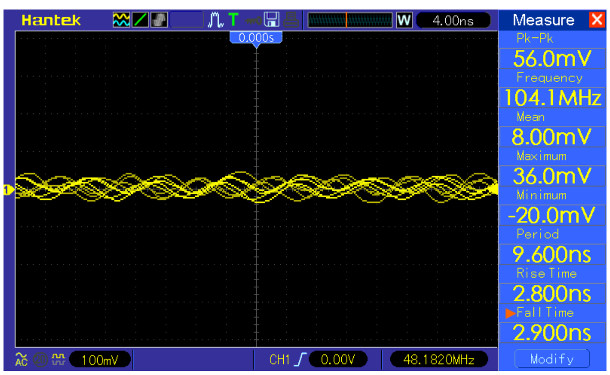

Fig. 3.3. Oscillation amplitude produced by recombining vertically polarized arm 2 and horizontally polarized arm 3 with LP1 and LP2 both set symmetrically at $\frac{\pi}{4}$ rad.

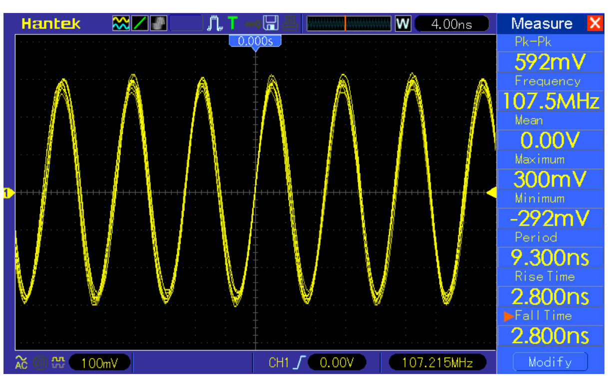

Fig. 3.4. Oscillation amplitude produced by recombining vertically polarized arm 2 and horizontally polarized arm 3 with LP1 and LP2 set anti-symmetrically, i.e. LP1 at $\frac{\pi}{4}$ rad and LP2 at $-\frac{\pi}{4}$ rad.

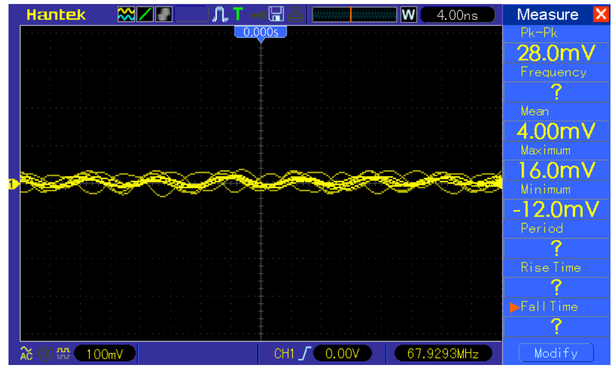

Fig. 3.5. Oscillation amplitude produced by recombining horizontally polarized arm 2 and vertically polarized arm 3 with LP1 and LP2 set symmetrically, i.e. LP1 at $\frac{\pi}{4}$ rad and LP2 at $\frac{\pi}{4}$ rad.

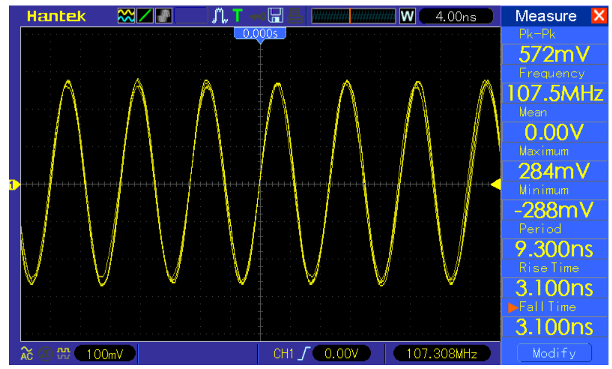

Fig. 3.6. Oscillation amplitude produced by recombining horizontally polarized arm 2 and vertically polarized arm 3 with LP1 and LP2 set anti-symmetrically, i.e. LP1 at $\frac{\pi}{4}$ rad and LP2 at $-\frac{\pi}{4}$ rad.

IV. THEORETICAL AGREEMENT

We begin the theoretical agreement analysis with defining an input state evolution step by step according to the ports notations shown on Fig.2. The source is a single coherent input in port 1 representing a normalized state 4-vector:

$$|\psi_{source}\rangle = \frac{1}{\sqrt{2}}\begin{pmatrix} \widehat{D}_{1,v}(\alpha_{1,v}) \\ 0 \\ \widehat{D}_{1,h}(\alpha_{1,h}) \\ 0 \end{pmatrix}|0\rangle \tag{13}$$

with $|0\rangle$ being a vacuum state, $\widehat{D}_{1,v}(\alpha_{1,v})$ and $\widehat{D}_{1,h}(\alpha_{1,h})$ being displacement operators [10] in spatial mode 1 in vertical and horizontal polarization modes accordingly. The action of PBS is represented by the matrix (14) which is CNOT gate in quantum computing [5]:

$$B_p = \begin{pmatrix} 1 & 0 & 0 & 0 \\ 0 & 1 & 0 & 0 \\ 0 & 0 & 0 & 1 \\ 0 & 0 & 1 & 0 \end{pmatrix} \tag{14}$$

hence, yielding:

$$|\psi_{PBS}\rangle \rightarrow B_p|\psi_{source}\rangle \rightarrow \frac{1}{\sqrt{2}}\begin{pmatrix}\widehat{D}_{2,v}(\alpha_{2,v})\\0\\0\\\widehat{D}_{3,h}(\alpha_{3,h})\end{pmatrix}|0\rangle \quad (15)$$

where $\widehat{D}_{2,v}(\alpha_{2,v})$ and $\widehat{D}_{3,h}(\alpha_{3,h})$ displacement operators in vertical and horizontal polarization modes shifted to spatial modes 2 and 3 accordingly. The phase modulation induced by the AOM is occurring in mode 3 and it is convenient to continue treating the diffracted beam which we selected for the recombination as spatial mode 3 as well. We derived the mode shifting for the diffracted beam using the function of phase modulation operator provided in [9], which adapted to our terms takes the following form:

$$\hat{S}_{PM} = \exp\left(\sum_1^\infty \hat{a}^\dagger_{\omega+\Omega} J_1(\omega)\hat{a}_\omega\right) \quad (16)$$

where: $\hat{a}_\omega$ is annihilation operator in the initial frequency mode of the source, $\hat{a}^\dagger_{\omega+\Omega}$ is creation operator in the AOM upshifted frequency mode and $J_1(\omega)$ is the first order Bessel function coefficient. It's worth adding a remark that expression of $\hat{S}_{PM}$ in the original paper contained a single-photon scattering coefficient instead of $J_1(\omega)$, however for a coherent state the expectation value of scattering coefficients summed over the infinity would plausibly result in $J_1(\omega)$. To show an action of the operator $\hat{S}_{PM}$ we represent the displacement operator $\widehat{D}_{3,h}(\alpha_{3,h})$ explicitly in a single frequency mode ω: $\widehat{D}_{3,h,\omega}(\alpha_{3,h,\omega})$. Now we apply $\hat{S}_{PM}$ transformation suggested in [9] upon the displacement operator which shifts it to frequency mode $\omega + \Omega$:

$$\hat{S}_{PM}\widehat{D}_{3,h,\omega}(\alpha_{3,h,\omega})\hat{S}^\dagger_{PM} = J_1(\omega)\widehat{D}_{3,h,\omega+\Omega}(\alpha_{3,h,\omega+\Omega}) \quad (17)$$

Using the equation (17) we can represent the state evolution as follows:

$$|\psi_{AOM}\rangle \rightarrow \frac{1}{\sqrt{2}}\begin{pmatrix}\widehat{D}_{2,v,\omega}(\alpha_{2,v,\omega})\\\hat{S}_{PM}\hat{a}_{3,v,\omega}\hat{S}^\dagger_{PM}\\\hat{a}_{2,h,\omega}\\\hat{S}_{PM}\widehat{D}_{3,h,\omega}(\alpha_{3,h,\omega})\hat{S}^\dagger_{PM}\end{pmatrix}|0\rangle \rightarrow$$

$$\frac{1}{\sqrt{2}}\begin{pmatrix}\widehat{D}_{2,v,\omega}(\alpha_{2,v,\omega})\\0\\0\\J_1(\omega)\widehat{D}_{3,h,\omega+\Omega}(\alpha_{3,h,\omega+\Omega})\end{pmatrix}|0\rangle \quad (18)$$

where: $\widehat{D}_{2,v,\omega}(\alpha_{2,v,\omega})$ is the displacement operator in vertical mode 2 and frequency ω; $\hat{a}_{3,v,\omega}$ and $\hat{a}_{2,h,\omega}$ are annihilation operators in vertical and horizontal modes 3 and 2 and frequency ω accordingly. Adhering to formalities we have indicated the action of $\hat{S}_{PM}$ on the operator $\hat{a}_{3,v,\omega}$ as phase modulation applies to all operators in spatial mode 3. The resulting state $|\psi_{AOM}\rangle$ acquires different frequency modes and it is not normalized any longer due to $J_1(\omega)$ coefficient. Now, as discussed in previous chapter in the pre-measurement sequence step 2 by adjusting the HWP1 we equalize amplitudes for modes 2 and 3 and normalize the state accordingly obtaining:

$$|\psi'_{AOM}\rangle \rightarrow \frac{1}{\sqrt{2}}\begin{pmatrix}\widehat{D}_{2,v,\omega}(\alpha_{2,v,\omega})\\0\\0\\\widehat{D}_{3,h,\omega+\Omega}(\alpha_{3,h,\omega+\Omega})\end{pmatrix}|0\rangle \quad (19)$$

The normalization is hence accounting for keeping the Bessel function coefficient $J_1(\omega)$ implicit throughout the derivation. It will also become apparent now why formalities with mode shifting were given in details when we consider the state in Schrödinger's picture, i.e. state $|\psi'_{AOM}\rangle$ evolving in time τ [11]:

$$|\psi'_{AOM}(\tau)\rangle \rightarrow \frac{1}{\sqrt{2}}\begin{pmatrix}\widehat{D}_{2,v,\omega}\left(\alpha_{2,v,\omega}(\tau)\right)\\0\\0\\\widehat{D}_{3,h,\omega+\Omega}\left(\alpha_{3,h,\omega+\Omega}(\tau)\right)\end{pmatrix}|0\rangle \rightarrow$$

$$\frac{1}{\sqrt{2}}\begin{pmatrix}e^{-i\omega\tau}\widehat{D}_{2,v,\omega}\left(\alpha_{2,v,\omega}(0)\right)\\0\\0\\e^{-i(\omega+\Omega)\tau}\widehat{D}_{3,h,\omega+\Omega}\left(\alpha_{3,h,\omega+\Omega}(0)\right)\end{pmatrix}|0\rangle \rightarrow$$

$$\frac{e^{-i\omega\tau}}{\sqrt{2}}\begin{pmatrix}\widehat{D}_{2,v,\omega}\left(\alpha_{2,v,\omega}(0)\right)\\0\\0\\e^{-i\Omega\tau}\widehat{D}_{3,h,\omega+\Omega}\left(\alpha_{3,h,\omega+\Omega}(0)\right)\end{pmatrix}|0\rangle \quad (20)$$

It is apparent from the expression (20) that we deduced the phase factor $e^{-i\Omega\tau}$, which will affect the oscillation dynamics of an observable – light intensity. The state (20) can be simplified by omitting common phase factor $e^{-i\omega\tau}$ in future calculations. Additionally, we can treat the coherent states in modes ω and $\omega+\Omega$ as fully tangential, i.e. $\langle\alpha_\omega|\alpha_{\omega+\Omega}\rangle = 1$, since physically our detection equipment is equally sensitive to these modes within the actual shift of ≈107 MHz for Ω. So, in further notations we can as well omit explicit indication of the frequency modes. Thus, we obtain the following normalized state:

$$|\psi'_{AOM}\rangle \rightarrow \frac{1}{\sqrt{2}}\begin{pmatrix}\widehat{D}_{2,v}(\alpha_{2,v})\\0\\0\\e^{-i\varphi}\widehat{D}_{3,h}(\alpha_{3,h})\end{pmatrix}|0\rangle \quad (21)$$

with φ being modulation phase $\varphi = \Omega\tau$. Using expression (21) we can define input states for test configurations. The action of HWP2 and HWP3 with FA set at $\frac{\pi}{4}$ is expressed in a matrix form using adapted Jones calculus definition [12], namely:

$$WP_2(\beta) = \begin{pmatrix} \cos 2\beta & 0 & \sin 2\beta & 0 \\ 0 & 1 & 0 & 0 \\ \sin 2\beta & 0 & \cos 2\beta & 0 \\ 0 & 0 & 0 & 1 \end{pmatrix} \qquad (22)$$

for the HWP2 with β being an angle of the wave-plate's FA and:

$$WP_3(\gamma) = \begin{pmatrix} 1 & 0 & 0 & 0 \\ 0 & \cos 2\gamma & 0 & \sin 2\gamma \\ 0 & 0 & 1 & 0 \\ 0 & \sin 2\gamma & 0 & \cos 2\gamma \end{pmatrix} \qquad (23)$$

for the HWP3 with γ being an angle of the wave-plate's FA. Hence, for the first test configuration we have the following input state:

$$|\psi_{in}^{I}\rangle \rightarrow WP_2\left(\frac{\pi}{4}\right)|\psi'_{AOM}\rangle \rightarrow \frac{1}{\sqrt{2}}\begin{pmatrix} 0 \\ 0 \\ \widehat{D}_{4,h}(\alpha_{4,h}) \\ e^{-i\varphi}\widehat{D}_{5,h}(\alpha_{5,h}) \end{pmatrix}|0\rangle \ (24)$$

where $\widehat{D}_{4,h}(\alpha_{4,h})$ and $\widehat{D}_{5,h}(\alpha_{5,h})$ are displacement operators in horizontal polarization mode shifted to spatial modes 4 and 5 accordingly. We will use the expression (12,c) as a test BS matrix for the purposes of showing worked example here. However, all of the four definitions (12,a-d) produce the same observables. Thus, we get the corresponding output state:

$$|\psi_{out}^{I}\rangle \rightarrow B|\psi_{in}^{I}\rangle \rightarrow \frac{1}{2}\begin{pmatrix} 0 \\ 0 \\ (1+e^{-i\varphi})\widehat{D}_{4,h}(\alpha_{4,h}) \\ (e^{-i\varphi}-1)\widehat{D}_{5,h}(\alpha_{5,h}) \end{pmatrix}|0\rangle \qquad (25)$$

Hence, the normalized intensity in port 4 oscillates as: $I_4^I(\varphi) = \left|\frac{1}{2}(1+e^{-i\varphi})\right|^2 = \cos^2\frac{\varphi}{2}$ and in port 5 as $I_5^I(\varphi) = \left|\frac{1}{2}(e^{-i\varphi}-1)\right|^2 = \sin^2\frac{\varphi}{2}$. The photocurrents generated by the correspondent PD's are directly proportional to these intensities: $j_4^I(\varphi) \sim I_4^I(\varphi)$ and $j_5^I(\varphi) \sim I_5^I(\varphi)$, so the PBD's output photocurrent is: $j_R^I(\varphi) = j_5^I(\varphi) - j_4^I(\varphi)$. In turn, the voltage oscillation that is observed on oscilloscope is directly proportional to the generated photocurrent. The actual proportionality constant is a function of: fraction of the beam area covering the PD's surface; PD's responsivity; LP's attenuation in transmission axis as well as impedance of an oscilloscope. Exactness of the constant estimation is, however, of no essence for this experiment as it scales equally for both polarization modes and we are only comparing the relative scaling factor for different configurations. Consequently, we represent the modeled voltage amplitude in arbitrary units in range $[-1,1]$ as a function of the photocurrent, i.e.: $V(j_R^I(\varphi)) = I_5^I(\varphi) - I_4^I(\varphi)$. Fig. 4 shows the plot of $V(j_R^I(\varphi))$ values out of full phase cycle $\varphi \in [0,2\pi]$:

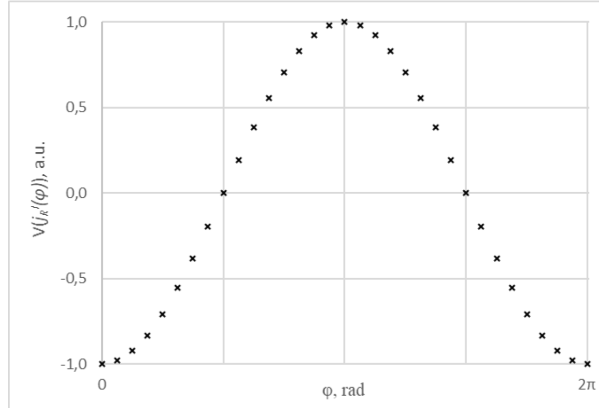

Fig. 4. Model of the voltage response in the test configuration 1.

Likewise, we model voltage of test configuration 2. The input state yields:

$$|\psi_{in}^{II}\rangle \rightarrow WP_3\left(\frac{\pi}{4}\right)|\psi'_{AOM}\rangle \rightarrow \frac{1}{\sqrt{2}}\begin{pmatrix} \widehat{D}_{4,v}(\alpha_{4,v}) \\ e^{-i\varphi}\widehat{D}_{5,v}(\alpha_{5,v}) \\ 0 \\ 0 \end{pmatrix}|0\rangle \ (26)$$

where $\widehat{D}_{4,v}(\alpha_{4,v})$ and $\widehat{D}_{5,v}(\alpha_{5,v})$ are displacement operators in vertical polarization mode shifted to spatial modes 4 and 5 accordingly. So, taking into account the polarization selectivity of dispersive prisms P1 and P2 we obtain:

$$|\psi_{out}^{II}\rangle \rightarrow B|\psi_{in}^{II}\rangle \rightarrow \frac{1}{2}\begin{pmatrix} 0.73(1-e^{-i\varphi})\widehat{D}_{4,v}(\alpha_{4,v}) \\ 0.73(1+e^{-i\varphi})\widehat{D}_{5,v}(\alpha_{5,v}) \\ 0 \\ 0 \end{pmatrix}|0\rangle \qquad (27)$$

where the $|\psi_{out}^{II}\rangle$ output state of the test configuration 2 is correlated to factor 0.73 so we can work in the same normalization scale for voltage response as in previous case. While one may suggest omitting the common factor 0.73 and consider the model normalization independently it may, however, appear confusing given the actual oscilloscope response. Thus, to have more quantitative approach we want to contrast the scales of all predicted models under the same normalization amplitudes. The factor 0.73 comes from $\sqrt{0.73}$ transmission amplitude for TE (vertical) mode per surface of dispersive prisms as discussed in experimental setup chapter. The resulting voltage $V(j_R^{II}(\varphi))$ oscillation plot is shown on Fig. 5.

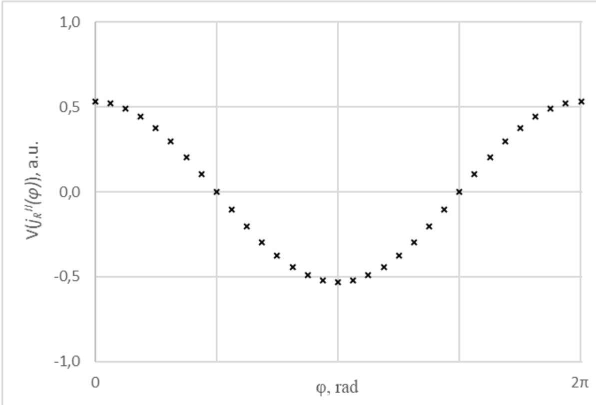

Fig. 5. Model of the voltage response in the test configuration 2.

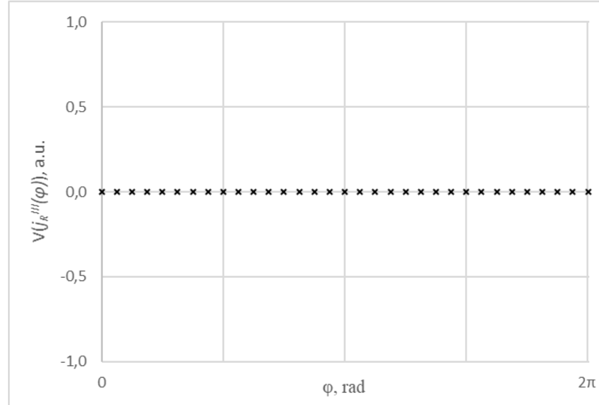

Fig. 6. Model of the voltage response in the test configuration 3.

In the third and fourth test configurations we use no waveplate but LP's with different angle settings. The effect of LP1 and LP2 can be defined according to the Jones calculus [12] as the following matrix suited for our 4-dimensional state vector:

$$LP(\theta_1, \theta_2) = \begin{pmatrix} \cos^2\theta_1 & 0 & \cos\theta_1 \sin\theta_1 & 0 \\ 0 & \cos^2\theta_2 & 0 & \cos\theta_2 \sin\theta_2 \\ \cos\theta_1 \sin\theta_1 & 0 & \sin^2\theta_1 & 0 \\ 0 & \cos\theta_2 \sin\theta_2 & 0 & \sin^2\theta_2 \end{pmatrix} \tag{28}$$

with θ_1 and θ_2 angles of transmission axes for LP1 and LP2 accordingly. Hence, in test configuration 3 we obtain:

$$|\psi_{in}^{III}\rangle \to |\psi'_{AOM}\rangle \tag{29}$$

$$|\psi_{out}^{III}\rangle \to LP\left(\frac{\pi}{4}, \frac{\pi}{4}\right) B |\psi_{in}^{III}\rangle \to$$

$$\frac{1}{4}\begin{pmatrix} 0.73(1+e^{-i\varphi})\widehat{D}_{4,\mathrm{v}}(\alpha_{4,v}) \\ 0.73(1+e^{-i\varphi})\widehat{D}_{5,v}(\alpha_{5,v}) \\ (1+e^{-i\varphi})\widehat{D}_{4,h}(\alpha_{4,h}) \\ (1+e^{-i\varphi})\widehat{D}_{5,h}(\alpha_{5,h}) \end{pmatrix} |0\rangle \tag{30}$$

where we can see the factor 0.73 cannot be omitted as it affects relative amplitudes. The expression (30) shows that all of four amplitudes are in phase, so by subtracting the intensities at port 4 and 5 which now have two components per port: $I_4^{III}(\varphi) = I_5^{III}(\varphi) = \left|\frac{0.73}{4}(1+e^{-i\varphi})\right|^2 + \left|\frac{1}{4}(1+e^{-i\varphi})\right|^2 = \frac{1+0.73^2}{4}\cos^2\frac{\varphi}{2}$ we obtain no oscillation for voltage $V(j_R^{III}(\varphi))$, Fig. 6.

In the same manner test configuration 4 output state becomes:

$$|\psi_{out}^{IIII}\rangle \to LP\left(\frac{\pi}{4}, -\frac{\pi}{4}\right) B |\psi_{in}^{IIII}\rangle \to$$

$$\frac{1}{4}\begin{pmatrix} 0.73(1+e^{-i\varphi})\widehat{D}_{4,\mathrm{v}}(\alpha_{4,v}) \\ 0.73(1-e^{-i\varphi})\widehat{D}_{5,v}(\alpha_{5,v}) \\ (1+e^{-i\varphi})\widehat{D}_{4,h}(\alpha_{4,h}) \\ (-1+e^{-i\varphi})\widehat{D}_{5,h}(\alpha_{5,h}) \end{pmatrix} |0\rangle \tag{31}$$

The voltage $V(j_R^{IIII}(\varphi))$ gives the following plot, Fig. 7.

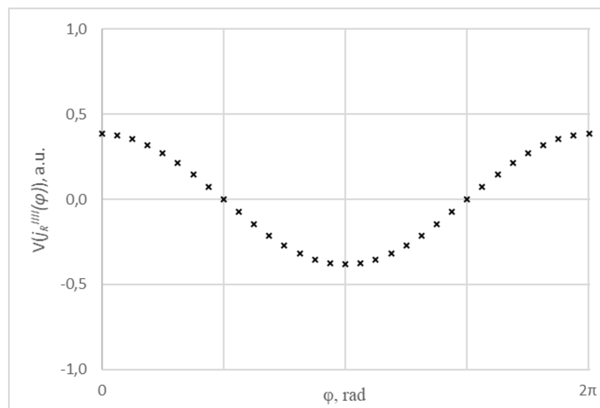

Fig. 7. Model of the voltage response in the test configuration 4.

For the input vectors $|\psi_{in}^{V}\rangle$ and $|\psi_{in}^{VI}\rangle$, i.e. of last two test configurations we perform a polarization state swap by applying both waveplate matrices upon vector $|\psi'_{AOM}\rangle$ (for which the order does not matter as these matrices commute):

$$|\psi_{in}^{V}\rangle = |\psi_{in}^{VI}\rangle \to WP_3\left(\frac{\pi}{4}\right) WP_2\left(\frac{\pi}{4}\right) |\psi'_{AOM}\rangle \to$$

$$\frac{1}{\sqrt{2}}\begin{pmatrix} 0 \\ e^{-i\varphi}\widehat{D}_{5,v}(\alpha_{5,v}) \\ \widehat{D}_{4,h}(\alpha_{4,h}) \\ 0 \end{pmatrix} |0\rangle \tag{32}$$

Thus, resulting output state for configuration 5 is:

$$|\psi_{out}^{V}\rangle \rightarrow LP\left(\frac{\pi}{4},\frac{\pi}{4}\right)B\left|\psi_{in}^{V}\right\rangle \rightarrow$$

$$\frac{1}{4}\begin{pmatrix} 0.73(-e^{-i\varphi}+1)\widehat{D}_{4,\mathrm{v}}(\alpha_{4,v}) \\ 0.73(e^{-i\varphi}-1)\widehat{D}_{5,v}(\alpha_{5,v}) \\ (-e^{-i\varphi}+1)\widehat{D}_{4,h}(\alpha_{4,h}) \\ (e^{-i\varphi}-1)\widehat{D}_{5,h}(\alpha_{5,h}) \end{pmatrix}|0\rangle \tag{33}$$

Hence, the fifth configuration gives the following voltage response, Fig. 8.:

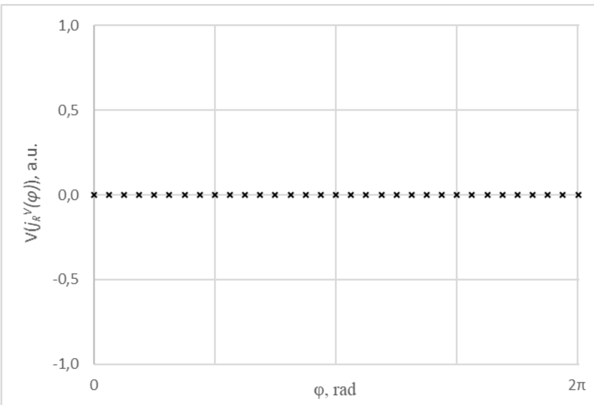

Fig. 8. Model of the voltage response in the test configuration 5.

Finally, in last configuration of the output state we apply the anti-symmetric position of LP's:

$$|\psi_{out}^{VI}\rangle \rightarrow LP\left(\frac{\pi}{4},-\frac{\pi}{4}\right)B\left|\psi_{in}^{VI}\right\rangle \rightarrow$$

$$\frac{1}{4}\begin{pmatrix} 0.73(-e^{-i\varphi}+1)\widehat{D}_{4,\mathrm{v}}(\alpha_{4,v}) \\ 0.73(e^{-i\varphi}+1)\widehat{D}_{5,v}(\alpha_{5,v}) \\ (-e^{-i\varphi}+1)\widehat{D}_{4,h}(\alpha_{4,h}) \\ (-e^{-i\varphi}-1)\widehat{D}_{5,h}(\alpha_{5,h}) \end{pmatrix}|0\rangle \tag{34}$$

And the corresponding voltage model is shown on Fig. 9.

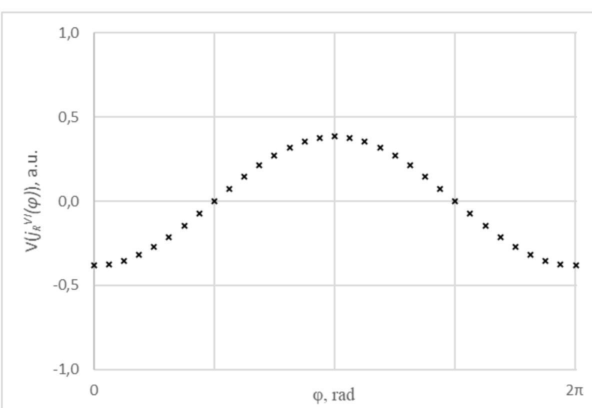

Fig. 9. Model of the voltage response in the test configuration 6.

We can now analyze an agreement of obtained models with respect to experimental data (Fig. 3.1-6.). This will require converting a.u. into volts. We begin with estimating the experimental error. The time series where no oscillation is modelled can be used to obtain an absolute value of error in measurement. Namely, we predicted 0 a.u. for any phase argument in test configurations 3 and 5, while experiment gives an oscillation depth of 56 mV and 28 mV in these tests respectively. Taking bigger value of 56 mV we see that signal deviates from 0 V at maximum by 36 mV. Thus, ± 36 mV can be used as an absolute error in measurement. Coming back to conversion of a.u. into volts we see that experimentally the maximum amplitude of 1.52 V was observed with the test 1. This result corresponds to the maximum amplitude among our theoretical models in a.u. as well. Therefore, we take 1.52 V as a reference for a maximum $[-1{,}1]$ a.u. oscillation range and consequently the depth of $|-1|+|1|=2$ a.u. Hence, for the test configuration 2 we have the depth of oscillation $|I_5^{II}(0)-I_4^{II}(0)|+|I_5^{II}(\pi)-I_4^{II}(\pi)|=|0.5329|+|-0.5329|=1.0658$, whereas 1.0658 scales to 2 as 0.810 V (to 3 s.f.) scales to 1.52 V. We immediately see that predicted 0.810 V agrees with the experimentally measured value of 0.816 V $\pm$ 36 mV for test 2. In a similar manner, we obtain predicted values for all configurations and provide a summary for their agreement with experimental in the following Table II.

TABLE II.
VERIFICATION OF THEORETICAL AGREEMENT WITH THE EXPERIMENTAL DATA

Test configuration	Theoretical prediction of the oscillation depth, a.u. (to 4 d.p.)	Theoretical prediction of the oscillation depth converted to volts with respect to 1.52 V, V (to 3 s.f.)	Experimental results of the oscillation depth with error in measurement, V (to 3 s.f.)
1	2	1.520	1.520 $\pm$ 36 mV
2	1.0658	0.810	0.816 $\pm$ 36 mV
3	0	0	0.056 $\pm$ 36 mV
4	0.7664	0.582	0.592 $\pm$ 36 mV
5	0	0	0.028 $\pm$ 36 mV
6	0.7664	0.582	0.572 $\pm$ 36 mV

V. CONCLUSIONS

We have discussed experimental and theoretical interference of classical fields in the Mach-Zehnder. Our theoretical predictions can as well apply to interference of light in a Fock state. Formalism-wise this can be easily seen if the displacement operators are exchanged with creation operators. In this case the interference statistics would be equivalent.

The experimental results agree with our theoretical predictions in each test apart from slight deviation in configuration 3 which amounts to about 3,5% respecting the reference voltage. Remarkably, the overall pattern of intensity correlations appears to be arguably trivial. One can see that intensities in ports 4 and 5 oscillate either completely in phase or completely out of phase featuring therefore a single phase permutation of π rad. Provided there was an ideal transmission for all the modes we would not need to account for any additional scaling factors and obtain only three different levels of oscillations. Thus, we would have: the maximum level for tests 1 and 2; exactly half of the maximum level for tests 4 and 6 due to absorption of diagonal components in linear polarizer and no oscillation for tests 3 and 5. Taking into account just these three levels the results could have been interpreted qualitatively (in phase/out of phase). Nevertheless, we opted for more quantitative analysis to avoid confusions in interpretation of experimental data.

Obtaining the correct correlations even qualitatively involves elaborate estimation of components in the beamsplitter matrix. Apparently, a common approach for a lossless reciprocal beamsplitter is insufficient. To give an example if we consider the following matrices:

$$\frac{1}{\sqrt{2}}\begin{pmatrix}1 & i & 0 & 0\\ i & 1 & 0 & 0\\ 0 & 0 & 1 & i\\ 0 & 0 & i & 1\end{pmatrix} \tag{35,a}$$

$$\frac{1}{\sqrt{2}}\begin{pmatrix}1 & 1 & 0 & 0\\ -1 & 1 & 0 & 0\\ 0 & 0 & 1 & 1\\ 0 & 0 & -1 & 1\end{pmatrix} \tag{35,b}$$

which completely satisfy the unitarity, i.e. conservation of energy/probability we would find that they provide wrong prediction for the correlations. E.g. both (35,a) and (35,b) predict an out of phase relation for tests 3 and 5 which is not the case in practice. This applies to all matrices in the theoretical setup chapter apart from expressions (12,a-d). The difference is that matrices (12,a-d) were derived with an additional quantum-mechanical condition. Namely, the orthogonality of polarization fields in physically separated output ports. By looking into the formalism of this condition (10) we see that it brings about a definite link between coefficients in different polarization and spatial modes. For instance, according to the expression (10), which can also be formulated as:

$$\langle \psi_{out_v} | \psi_{out_h} \rangle = \langle c_v | c_h \rangle + \langle d_v | d_h \rangle = 0 \tag{36}$$

we require the identity (11,a): $(t^2 + \tilde{r}_v^* \tilde{r}_h) a_v^* a_h = 0$ to hold. In turn, the term $t^2 a_v^* a_h$ emerges from $\langle c_v | c_h \rangle$ and the term $\tilde{r}_v^* \tilde{r}_h a_v^* a_h$ from $\langle d_v | d_h \rangle$, i.e. inner products of spatially separated modes. Without making any far-fetched claims this relation seems to be non-locally correlated at least in Hilbert space representation. And philosophy behind it is as follows – beamsplitter should not know upfront how to exactly portion amplitudes for different modes being a random optical device. From stand point of classical electromagnetism such orthogonality is clearly trivial and would not require any particular rules like (11,a-d). Yet, we could experimentally confirm that (11,a-d) should be observed even in case of classical fields.

Interestingly, the matrices (12,a-d) also predict phase complementarity for the intensities of orthogonal fields. The prediction for out of phase oscillation can be seen by superposing the graphs from Fig. 4 and Fig. 5 as well as those from Fig. 7 and Fig. 9. This suggests that by running the tests 1 and 2 simultaneously we should see how their intensity phases alternate. In practice we are unable to verify this as it is out of scope of our experimental equipment.

All in all, where would such precision of a beamsplitter 4-matrix even matter? We argue that it matters to practically achieve an increase in processing power of photonic quantum computers. In particular, we investigated a beamsplitter which performs a transformation into superposition of four different states – a 4-dimensional photonic Hadamard gate. An increase in processing power can be evident if we consider linear quantum computer circuits discussed in [14]. By implementing such Hadamard gates into the circuits we expand total dimensions per component to four and hence practically obtain a 4-dimensional qubit. This actually quadruples processing power with respect to a 2-dimensional qubit.

Appendix I

To model the Hong-Ou-Mandel effect let us consider a state of two left circularly polarized [12] photons each entering different ports:

$$|\Psi_{in}\rangle = \frac{1}{2}\begin{pmatrix}1\\ 1\\ i\\ i\end{pmatrix} \tag{A}$$

then using (12,a) for *B* we obtain the following state:

$$|\Psi_{out}\rangle = B|\Psi_{in}\rangle = \frac{1}{2\sqrt{2}}\begin{pmatrix}1-i\\ 1-i\\ i-1\\ i-1\end{pmatrix} \tag{B}$$

where we can see that amplitudes with the same polarization always cancel out, so in fact the model returns coalescence in polarization. To verify this experimentally the HOM experiment should be fitted with optical instruments allowing polarization control.

Acknowledgment

We thank Rob Sunderland from the Niels Bohr Institute for inspirational quantum talk and Alexander Franzen for making the optical components library for the Inkscape graphical editor to make the drawing of experimental setup.

References

[1] Petr Kučera, “Quantum Description of Optical Devices Used in Interferometry”, Radioengineering, Vol. 16, No. 3, September 2007, p. 4,5.

[2] Daniel J. Lum, Samuel H. Knarr, and John C. Howell, "Fast Hadamard transforms for compressive sensing of joint systems: measurement of a 3.2 million-dimensional bi-photon probability distribution," Opt. Express 23, 27636-27649 (2015), p. 5,6.

[3] Zibang Zhang, Xueying Wang, Guoan Zheng, and Jingang Zhong, "Hadamard single-pixel imaging versus Fourier single-pixel imaging," Opt. Express 25, 19619-19639 (2017).

[4] Mark B. Schneider and Indhira A. LaPuma, “A simple experiment for discussion of quantum interference and which-way measurement”, Am. J. Phys. 70 (3), March 2002.

[5] G. Weihs, A. Zeilinger, “Photon statistics at beam-splitters: an essential tool in quantum information and teleportation, Coherence and Statistics of Photons and Atoms", J. Perina (Ed.), Wiley, (2001), p. x.
[6] Z. Y. Ou, and L. Mandel, “Derivation of reciprocity relations for a beam splitter from energy balance”, American Journal of Physics, Vol. 57, (1989), p. 67.
[7] AA OPTO-ELECTRONIC, “Acousto-optic Theory Application Notes”, 2013. p. 3. Available: http://www.aaoptoelectronic.com/wp-content/uploads/documents/AAOPTO-Theory2013-4.pdf
[8] Thorlabs, N-SF11 Equilateral Dispersive Prisms (420 nm - 2.3 µm), Available: https://www.thorlabs.com/newgrouppage9.cfm?objectgroup_id=148
[9] José Capmany and Carlos R. Fernández-Pousa, "Quantum model for electro-optical phase modulation," J. Opt. Soc. Am. B27, A119-A129 (2010), p.12.
[10] L. Mandel and E. Wolf, “Optical coherence and quantum optics”, Cambridge University Press (1995), p. 526, 527.
[11] Allan Adams, “Lecture 6 Time Evolution and the Schroedinger Equation”, Quantum Mechanics, MIT, 2013, p. 8.
[12] J. Peatross and H. Stokes, “Physics of Light and Optics”, 2001, pp. 65-70.
[13] C.K. Hong, Z.Y. Ou, and L. Mandel, “Measurement of Subpicosecond Time Intervals between Two Photons by Interference”, Physics Letters, Vol. 58 (18), 1987.
[14] E. Knill, R. Laflamme and G. J. Milburn “A scheme for efficient quantum computation with linear optics” Nature, Vol. 409, 4 January 2001.